analytical chemistry

Article

pubs.acs.org/ac

Detection of miRNA Using a Double-Strand Displacement Biosensor with a Self-Complementary Fluorescent Reporter

Nicholas E. Larkey,[†] C. Kyle Almlie,[†] Victoria Tran,[†] Marianne Egan,[‡] and Sean M. Burrows*[,†]

[†]Department of Chemistry, Oregon State University, 153 Gilbert Hall, Corvallis, Oregon 97331, United States

[‡]School of Design and Human Environment, Oregon State University, 230 Milam Hall, Corvallis, Oregon 97331, United States

Supporting Information

ABSTRACT: Design of rapid, selective, and sensitive DNA and ribonucleic acid (RNA) biosensors capable of minimizing false positives from nuclease degradation is crucial for translational research and clinical diagnostics. We present proof-of-principle studies of an innovative micro-ribonucleic acid (miRNA) reporter-probe biosensor that displaces a self-complementary reporter, while target miRNA binds to the probe. The freed reporter folds into a hairpin structure to induce a decrease in the fluorescent signal. The self-complementarity of the reporter facilitates the reduction of false positives from nuclease degradation. Nanomolar limits of detection and quantitation were capable with this proof-of-principle design. Detection of miRNA occurs within 10 min and does not require any additional hybridization, labeling, or rinsing steps. The potential for medical applications of the reporter-probe biosensor is demonstrated by selective detection of a cancer regulating microRNA, Lethal-7 (Let-7a). Mechanisms for transporting the biosensor across the cell membrane will be the focus of future work.

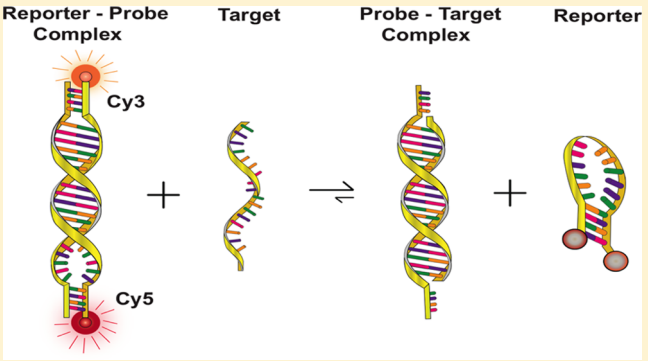

Expression of micro-ribonucleic acid (miRNA) has been associated with the regulation and progression of numerous cancers such as breast,[1−3] thyroid,[4,5] colorectal,[6,7] prostate,[8,9] lung,[10,11] and ovarian.[12,13] While miRNAs are critical in the regulation of cancers, many other diseases such as cardiovascular diseases,[14] neurological diseases,[15] and immunological diseases[16] also exhibit miRNA-based regulation. Monitoring changes in miRNA biomarkers can be used to signify the early onset of disease. However, miRNAs are usually present in the nanomolar to femtomolar concentration range.[17] Therefore, screening for miRNA requires the use of methods with high sensitivity, such as quantitative reverse-transcriptase polymerase chain reaction (qRT-PCR),[18,19] microarrays,[1,17,20,21] and Northern blotting.[19,22−25] These methods are ideal for cell lysates but not *in situ* cellular analysis. Current biosensors for *in situ* cellular analysis include: molecular beacons,[26−29] dual molecular beacons,[30−32] dual linear probes,[33−35] intercalator biosensors,[36−38] double-strand displacement biosensors,[39,40] NanoFlares,[41] and molecular sentinels.[42,43] In general, these methods provide selectivity and high sensitivity but suffer from slow analysis, false positives, or a lack of high selectivity. A majority of oligonucleotide-based fluorescent biosensors demonstrate an increase of fluorescence intensity upon target binding by disrupting a quenching mechanism. When these biosensors are used for *in situ* cellular analysis, they suffer from false positives because nucleases can cleave either the fluorophore or the quencher from the oligonucleotide strand(s). False positives diminish the detection sensitivity and imaging contrast for cellular analysis. In order to reduce false positives, the change in luminescent signal must occur by bringing together molecules that will interact with one another to change spectral response. We present a new approach for luminescent biosensors that combines the attributes of locked nucleic acids, speed, selectivity, sensitivity, and low false positives to overcome the limitations in the field.

Our approach to improve RNA sensing technology involves a target RNA displacing a self-complementary reporter from a reporter-probe complex (Scheme 1). Self-complementarity of the reporter causes it to fold into a hairpin configuration upon displacement from the probe. This forces two dyes at distal ends of the reporter together, accommodating intermolecular energy coupling mechanisms that govern the change in the analytical signal and consequently aid in reducing false positives. The reporter and probe are only partially complementary but stable at room temperature with a melting temperature of 39 °C. The full complementarity of the probe and target form a more thermodynamically stable complex at room temperature with a melting temperature of 54 °C. This condition drives the reaction in Scheme 1 to the right.

Dual molecular beacons and dual linear probes reduce enzymatic-related false positives, but both require a three to four nucleotide gap in-between adjacent oligonucleotide

Received: November 27, 2013
Accepted: January 13, 2014
Published: January 13, 2014

   dx.doi.org/10.1021/ac403866g | *Anal. Chem.* 2014, 86, 1853−1863

Scheme 1. Schematic of Recognition Mechanism

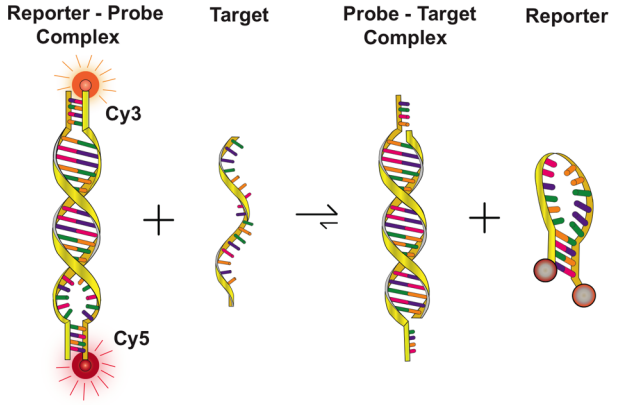

sensing strands.[30−35] This gap, needed to reduce steric hindrance between the two sensing strands upon target binding, creates two potential problems: (1) true single nucleotide polymorphism (SNP) specificity cannot be realized without exhaustive optimization of the dual sensing strands and (2) stable binding to short 19 to 22 nucleotide RNAs will be thermodynamically difficult. Dual linear probes further suffer from nonspecific binding issues compared to dual molecular beacons.[30,31,33−35] The reporter-probe biosensor presented here has great potential to provide improved selectivity and stronger binding to target miRNA over dual sensing strand designs because the unlabeled probe is fully complementary to the target.

In this work, we present proof-of-principle studies of a reporter-probe displacement biosensor capable of selectively detecting a cancer regulating miRNA, Lethal-7 (Let-7a). We used Let-7a because the Let-7 family is highly conserved across many animal species and has been linked to cell-based diseases.[44−49] The reporter-probe displacement biosensor presented here combines the positive attributes of competitive binding with a change in luminescence from intramolecular binding to provide high selectivity and reduce false positives. The complexation thermodynamics, two-photon characteristics, spectral properties, binding kinetics, binding selectivity, analytical figures of merit, and extent of false positives for the reporter-probe biosensor are discussed. The reporter-probe biosensor is an attractive alternative to current biosensors because nanomolar amounts of miRNA were detected within 10 min of hybridization. In addition, false positives were reduced by more than 20% compared to molecular beacons.

EXPERIMENTAL SECTION

Single- and Two-Photon Spectral Characteristics of the Reporter. The reporter is an oligonucleotide with a cyanine-3 dye (Cy3) on the 3-prime end and a cyanine-5 dye (Cy5) on the 5-prime end. These dyes were selected for their energy coupling prospects. Excitation and emission spectra of the reporter in the hairpin and open configurations were recorded. Working solutions of the reporter, reporter-probe, and reporter-probe plus target were prepared to contain approximately 1 μM of each reagent. Similar solutions were used to investigate the linearity and nonlinearity of photon absorption of the reporter in both the hairpin and open configurations. A more detailed description of the reporter and probe sequence and configuration will be discussed below and presented in Table 1.

Figure 1 is a diagram of the custom-built fluorimeter used for characterization of the reporter-probe displacement biosensor. A Titanium-Sapphire (Mai Tai, Spectra Physics, Newport) laser produced 100 femtosecond (fs) long pulses at a repetition rate of 80 MHz. The Mai Tai laser wavelength is tunable from 690 to 1040 nm. The excitation beam reflects off a mirror and passes through a half-wave-plate and Glan-polarizer (Newport) to control the power. A beam sampler (Newport, 10B20-01NC.2) reflects ∼4% of the excitation beam to a photodiode (Newport, 918D-SL-OD3R) to monitor and control the power. The transmitted beam continues to a second mirror (Newport, 10Q20UF.35P) to be directed through a 705 nm long-pass dichroic beam splitter (Semrock, FF705-Di01-25x36). After passing through the dichroic, the laser beam is focused into a cuvette using a 25 mm focal length plano-convex lens (Newport, KPX076 AR.16). Emission from the sample is collected with the same lens used to focus the excitation beam. The emission beam is reflected by the dichroic mirror and

Table 1. Oligonucleotide Sequences and Predicted Thermodynamic Complexation Values[a]

name	sequence (5′-3′)	Gibbs energy (kcal/mol) target	nonsense	reporter
Reporter	Cy5/CATCGTTGAATAC+**TAGGTTGT+ATAGT**TCGAT+G/Cy3Sp	−3.2	−6.2	
Reporter (No Cy3)	Cy5/CATCGTTGAATAC**TAGGTTGTATAGT**TCGATG	−3.2	−6.2	
Probe1	**ACTATACAACCTACTACCTC**	**-23.0**	−2.5	**-13.1**
Probe2	CATCG**TACTATACAACCTACTACCTCA**CGATG	**-24.7**	−2.5	**-19.5**
Let-7a Target	**U*GA*GGmUAmGUAGGUUmGUmAU*AGU*U**			−3.2
Let-7a Variation (Let-7aV)	**U*GA*uGUAcaAGGUUGUAU*AGU*U**			−3.3
miR-9 Nonsense	U*CA*UAmCAmGCUAGAUmAAmCC*AAA*GA	−5.7		−6.2
Molecular Beacon	Cy5/TCATC**GAACTATACA+ACCTACTAC+CTCAC**GAT+GA/IAbRQSp	**-25.4**	−2.9	
Cy3-linear Reporter	**AACTATACAACCTACTACCTCA**/Cy3Sp			
Cy5-linear Reporter	Cy5/**TGAGGTAGTAGGTTGTATAGTT**			

[a]All thermodynamic values were obtained using software available from The DINAMelt Web Server[51−53] managed by The RNA Institute at SUNY-Albany. The "Two State melting (hybridization)" function was used for double-strand binding calculations. Experimental parameters used for thermodynamic calculations were: 25 °C, 10 mM Na^+, 2.5 mM Mg^{2+}, and 1 μM oligonucleotide. Calculations could not incorporate added stability provided by chemical modifications. Bold sections of the sequences refer to complementary binding sites. Underlined sections depict complementary regions of the stems for the reporter, probe2, and molecular beacon. The bold thermodynamic values correspond to significant complexation reactions. (+) symbol represents location of locked nucleic acid. (*) symbol represents location of a phosphorothioated modification. (m) symbol represents location of a 2′O-methyl modification.

dx.doi.org/10.1021/ac403866g | Anal. Chem. 2014, 86, 1853−1863

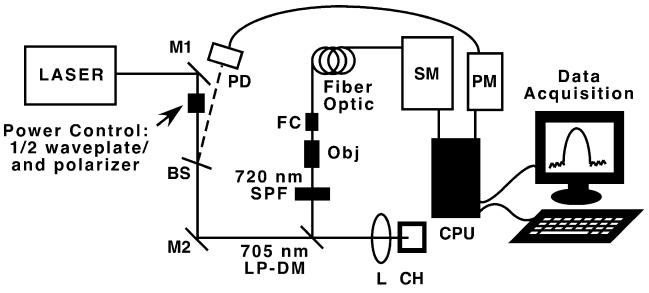

Figure 1. Experimental apparatus. Laser = Mai Tai (690 to 1040 nm); M1 = Mirror1, M2 = Mirror2, BS = Beam Sampler, PD = Photo Diode, LP-DM = 705 nm Long-Pass Dichroic Mirror, L = 25 mm Focal Length Lens, CH = Cuvette Holder, SPF = 720 nm Short-Pass Filter, Obj = Objective (10×, 0.25 NA), FC = Fiber Coupler, SM = Spectrometer, PM = Power Meter, and CPU = Central Processing Unit.

passes through a 720 nm short-pass filter (Semrock, FF01-720/SP-25) to remove any backscattered photons from the source. A 10×, 0.25 Numerical Aperture (NA) objective focuses the emission beam into a 2 m long fiber optic (Ocean Optics, QP1000-2-VIS-NIR). The fiber optic connects to a QE65 Pro spectrometer (Ocean Optics). For experiments using the QE65 Pro, the charge coupled device (CCD) was thermoelectrically cooled to −20 °C to reduce dark noise. The spectrometer has a grating with 1200 grooves/mm and a spectral range from 520 to 690 nm. For sensitivity and limit of detection characterization of the biosensor, we used an Acton Spectrometer (SP-2356) containing a grating with 300 grooves/mm blazed at 500 nm (Princeton Instruments). An electron-multiplied CCD (Princeton Instruments, 512B-eX-celon3-EMCCD) was used as the detector. Acquisition parameters depended on the concentration of reporter-probe complex. The slit width, grating center, and CCD temperature were constant at 1000 μm, 650 nm, and −70 °C. The spectral window ranged from 613.3 to 698.1 nm. Such a grating position minimized spectral interference from residual scatter from the excitation source that was not removed by the dichroic mirror and short pass spectral clean up filter.

The wavelength from the Mai Tai was controlled using the Mai Tai GUI program (Spectra Physics, Newport). As mentioned previously, the Mai Tai laser power is controlled with a half-wave-plate and a Glan-polarizer. Rotation of the half-wave plate with respect to the Glan-polarizer allows precise control of the average power at the sample. The rotation of the half-wave-plate is controlled by software available from Newport (CCVA-PR). A power meter (Newport, 1918-R) measured the average power of the reflected excitation beam at the photodiode. Assuming no absorption by the beam sampler, the Newport software mentioned above also calculates transmitted power using the Fresnel equation[50] and the measured reflected laser power. Spectral emission data was collected and stored using either SpectraSuite software from Ocean Optics or Lightfield from Princeton Instruments. All experimental data was processed using custom-written Matlab algorithms.

To confirm emission characteristics observed using the pulsed source, we conducted experiments using a continuous wave source. The continuous-wave experiments use a diode pumped solid-state laser (Gem, LaserQuantum) operating at 532 nm. The same type of fiber optic coupler and QE65 Pro spectrometer described previously were also used for continuous-wave experiments.

Oligonucleotides and Materials. Oligonucleotides were purchased from Integrated DNA Technologies and Exiqon and used as received. Only probe1 was purchased from Exiqon. Oligonucleotide sequences and predicted thermodynamic data are shown in Table 1. Open-source software available on the DINAMelt Web Server[51−53] was used to calculate all the thermodynamic data presented in Table 1. The reporters and probes were made out of DNA and locked nucleic acids (LNA). The miRNA have a 2′O-methylation and/or a phosphorothiolation modification to improve long-term stability of the oligonucleotide. The 2′O-methylation of the miRNA adds a methyl group to the 2′hydroxyl group of the ribose moiety. Phosphorothiolate bond modification substitutes a sulfur atom for a nonbridging oxygen on the phosphate backbone of an oligonucleotide. The reporter was designed to contain three strategically placed LNAs. The probe sequence contained patent protected placement of LNAs (Exiqon, 4100170-00). LNAs help stabilize the oligonucleotide against nuclease degradation by implementation of a carbon bridge between the 4′ carbon and the 2′ oxygen of the ribose moiety. Use and determination of optimum placement of LNA to reduce false positives can be cost-prohibitive. Furthermore, recent studies have found LNA to have a toxic effect to some cell lines.[54] The reporter-probe biosensor presented here uses LNA in low concentration to limit toxicity. LNA-LNA form stronger intermolecular bonds than LNA-DNA and LNA-RNA bonds. Since double strand displacement mechanisms usually use more complementary base pairs than molecular beacons, getting displacement to occur will be difficult if too many LNAs are needed to minimize false positives. We suggest that the reporter-probe biosensor adds an extra level of rejection to false positives and can help reduce cost. Future reporter-probe designs will explore the need for LNA modifications. If LNA do not contribute to reducing false positives, then the reporter-probe could be free of LNA and reduce a potential source of toxicity of the biosensor.

Tris buffer (pH 10), Tween 20, phosphate buffered saline (PBS, pH 7.0), and 2 M magnesium chloride ($MgCl_2$) were obtained from Fisher Scientific and used as received. Stock solutions of all oligonucleotides were prepared with 18 MΩ RNase-free water (complements of the Remcho Lab at Oregon State University). Working solutions of oligonucleotides were prepared using a buffer solution containing 10 mM Tris buffer, 2.5 mM $MgCl_2$, and 0.005% Tween 20 in PBS. The final pH of the buffer solution was approximately 8. Concentrations of oligonucleotides were verified using a Nanodrop spectrometer (Thermo Scientific, ND-1000 UV−vis Spectrometer).

Binding Kinetics and Analytical Signal Dynamics. To confirm selectivity of the reporter-probe biosensor, the analytical signals from the reporter were observed before and after *in situ* addition of probe, target Let-7a, or non-complementary miR-9. The signal change was observed in real time to track how different reagent additions changed the analytical signal and to monitor signal stability. These experiments started with the reporter in the hairpin configuration to establish a starting point for Cy3 and Cy5 emission intensities. The reporter-probe complex was formed by incubation of the reporter with probe for 20 min at room temperature. A 10 min incubation period was used after addition of either target or noncomplementary miRNA to the reporter-probe biosensor. Dilution controls involved sequential addition of buffer to the reporter. These controls were used to determine dilution factors and confirm signal changed according to dilution factor.

dx.doi.org/10.1021/ac403866g | *Anal. Chem.* 2014, 86, 1853−1863

Preliminary studies of the change in analytical signal were carried out with working solutions containing approximately 1 μM of reporter. Addition of probe resulted in a solution of 833 nM reporter and 833 nM probe. Addition of target Let-7a, Let-7a variant (Let-7aV), or miR-9 produced solutions containing 750 nM reporter, 750 nM probe, 750 nM target Let-7a, 750 nM Let-7aV, or 750 nM miR-9. Dilution control solutions were prepared by successive addition of buffer to the 1 μM reporter solution to dilute it to 833 and 750 nM. The same dilution protocol was used when a reporter without Cy3 had its signal change analyzed.

Analytical signal intensity was acquired for 1 min time intervals every 5 min over at least 30 min. Each 1 min signal acquisition consisted of 6 replicate measurements of a 10 s exposure time. The average Let-7aV signal included cuvette placement error by repositioning the cuvette after each 1 min exposure time, and the signal was monitored over a 5 min period. The laser beam was blocked during incubation times and in-between time-point measurements to minimize photodamage of oligonucleotides and the dyes. All average signal counts are background corrected.

Cell Lysate Protocol. DH10b *E. coli* cells were cultured to saturation in 2×YT (yeast extract tryptone) media at 37 °C and gently shaken at 250 rpm. Cells were centrifuged at 5000 rpm for harvesting, and a 50 μL aliquot of cells was stored in a −80 °C freezer. On the day the cell lysate was needed, a sample of cells was taken out of the freezer and thawed at room temperature. The cells were resuspended in 50 mL of dilution buffer and lysed at 18 000 psi with a Microfluidizer (Microfluidics M-110P) at 0 °C. The cell lysate was then centrifuged at 20 000 relative centrifugal force for 20 min. Finally, the supernatant lysate passed through a 0.20 μm filter to remove large cell debris and maintain DNA, RNA, proteins, and other cell lysate materials. The filtered cell lysate was then diluted in half using buffer solution described above. The half-diluted cell lysate solution was then used to look for interferences in biosensor response in the presence of cell debris. Buffer controls were performed in parallel with cell lysate studies for comparison of the reporter's response in each type of environment. Reporter at 1 μM was analyzed before the addition of either diluent or probe to reduce the concentration to 833 nM. After 10 min of hybridization, the solution was analyzed. Then, either another addition of diluent or Let-7a was added. After a 20 min incubation period, the solution was analyzed. This solution contained 750 nM probe-Let-7a and reporter. As described above, the signal from the reporter was collected over a 1 min period. Each signal acquisition consisted of 6 replicate measurements with a 10 s exposure time. After each 1 min exposure time, the cuvette was repositioned three times to incorporate cuvette placement error into the average signal.

Analytical Figures of Merit. Reporter-probe complex solutions were prepared by incubating equimolar amounts of reporter and probe for one hour. All standard solutions were prepared to contain either 1 μM or 100 nM reporter-probe complex. The sensitivity of the 1 μM reporter-probe complex was evaluated using standard solutions containing 0, 5, 25, 125, 250, 500, 750, and 1000 nM of Let-7a. The 100 nM reporter-probe complex standard solutions contained 0, 1, 5, 10, 25, and 50 nM Let-7a. After addition of Let-7a to the reporter-probe complex, the solutions were allowed to hybridize for at least 1 h prior to analysis.

For sensitivity evaluations, the changes in fluorescence of the standard solutions were analyzed using a 300 mm focal length spectrometer (Acton SP-2356 spectrometer, Princeton Instruments, 300 grooves/mm grating) equipped with an electron-multiplied charge coupled device (ProEM 512B-eXcelon3-EMCCD, Princeton Instruments). The fiber optic delivering fluorescence to the spectrometer had a 1000 μm core diameter and was placed directly at the entrance slit of the spectrometer. To optimize light throughput, the spectrometer slits were opened to 1000 μm in order to match the core diameter of the fiber.

Various data acquisition parameters were evaluated for optimal signal-to-noise and detector response sensitivity. Optimum acquisition parameters for the 1 μM reporter-probe complex were: 100 ms exposure time, low noise analog to digital conversion, 100 kHz full frame readout rate, and high analog-to-digital conversion gain. For the 100 nM reporter-probe complex, only the exposure time was increased to 500 ms. To improve signal-to-noise and establish instrumental error, ten exposures were averaged and six replicates were taken. After the six replicates were taken, the cuvette was repositioned three times and the acquisition process was repeated. This procedure allowed cuvette placement error to be determined. The samples were excited with 742 nm at 75 mW average power.

False Positives from Nuclease Degradation. Solutions of reporter-probe complexes, molecular beacons, and double-strand displacement biosensors were tested for false positive signal generation. An endonuclease degradation procedure was adapted from the Promega RT-PCR DNase treatment protocol. The enzyme solution containing endonuclease was added to the samples in excess and then incubated at 37 °C for 30 min. RQ1 DNase stop solution was added to the solutions and incubated at 65 °C for 10 min. Each solution was then diluted to approximately 833 nM of oligonucleotide biosensor of interest. Control solutions without nucleases only contained the nucleic acids of interest at equivalent concentrations to those in the endonuclease test solutions. The control solutions were not heated or treated to endonucleases. Solutions containing the endonuclease were analyzed for an increase or decrease in signal intensity compared to their respective control solutions.

RESULTS AND DISSCUSSION

Thermodynamic Considerations for the Recognition Mechanism. Thermodynamic stability of the reporter-probe complex governed whether or not a potential target would displace the reporter. The reporter-probe complex is designed to be resistant to nonspecific binding; however, presence of a complementary target miRNA will disrupt the reporter-probe complex to form a more thermodynamically stable probe-target complex, freeing the reporter in the process. The freed reporter uses intramolecular binding to fold into a hairpin configuration. This intramolecular binding event is used to force the donor and acceptor resonant energy pairs into close proximity to cause a change in the analytical signal. The reporter behaves similarly to a reverse molecular beacon (rMB)[55,56] but differs in that the reporter presented here works at room temperature and is not complementary to the target miRNA. Scheme 1, discussed in the introduction, shows the recognition mechanism for the reporter-probe biosensor.

Key Gibbs energy values are reported in Table 1 and highlighted in bold. Two probe designs were investigated; probe1 with partial complementarity to the loop region of the reporter and probe2 with partial complementarity to the loop and stem regions of the reporter. Both probe1 and probe2 are designed to be fully complementary to Let-7a. The Gibbs

energies of reporter-probe1 and reporter-probe2 complex are −13.1 and −19.5 kcal/mol, respectively. The Gibbs energies for probe1-target and probe2-target complex are −23.0 and −24.7 kcal/mol, respectively. The more negative Gibbs binding energy of the probe-target complex drives the reaction to form probe-target complexes and free reporters. Table 1 also shows that potential nonspecific binding interactions have non-favorable thermodynamic values. These values demonstrate the reporter-probe complex is indeed more stable than any potential nonspecific complexation. All values were obtained using the Two State melting (hybridization) application available from The DINAMelt Web Server available at The RNA Institute at SUNY-Albany.[52−54]

If the reporter-probe biosensors are to be used at 37 °C, then the binding thermodynamics would need to be re-evaluated. By tuning the nucleic acid sequence of the reporter, the binding thermodynamics can be adjusted to demonstrate competitive binding at other temperatures. There will also be other competing binding mechanisms with nonspecific species that need to be accounted for at the different operating temperatures.

Transduction Mechanism. The reporter has Cy3 and Cy5 fluorophores located at the distal ends of the oligonucleotide strand. Table 1 lists the dye and oligonucleotide configuration of the reporter. Figure 2 shows the fluorescent transduction mechanism of the reporter-probe1 biosensor. The emission in Figure 2 resulted from excitation of the reporter at 742 nm with approximately 100 mW of average power. The hairpin configuration of 1 μM reporter has a maximum emission from Cy5 at 670 nm with approximately 8000 counts per 10 s (blue line, Figure 2a). Complexation of 1 μM probe1 with 1 μM reporter causes the Cy5 signal to increase to about 18 000 counts per 10 s (green dash, Figure 2a). When 1 μM reporter, 1 μM probe1, and 1 μM Let-7a are added together, the Cy5 signal returns to approximately 7000 counts per 10 s (red dash-dot, Figure 2a). Addition of probe1 caused the Cy5 signal to increase by ∼10 000 counts per 10 s compared to the Cy3 signal increase of ∼100 counts per 10 s (Figure 2). Thus, emission from Cy5 is the dominant contributor to the reporter's analytical signal.

Figure 2 demonstrates the current reporter-probe displacement biosensor behaves as a signal-off type biosensor. To confirm the reduction in signal was from the folding of the reporter into a hairpin and not an artifact from the ultrafast laser, we used a continuous-wave laser to look at the signal dynamics. Samples containing reporter, reporter-probe1, and reporter-probe1 plus target were excited with 532 nm laser irradiation from the Gem laser at ∼3.4 mW. Emission spectra from the continuous-wave source confirmed the reporter-probe1 displacement biosensor decreased the Cy5 and Cy3 emission when the reporter was in the hairpin configuration (Figures S1 and S2, Supporting Information).

The signal from the solutions containing only reporter (blue line, Figure 2) and the reporter-probe1 plus Let-7a (red dash-dot, Figure 2) should be approximately the same because both contain 1 μM of the reporter in the hairpin configuration. We found that the ∼10% difference in signal between the two solutions was from cuvette placement. Examination of the relative standard deviation of the reporter's average summed intensity from cuvette placement experiments revealed a 1.7% to 8.8% error (data not shown). The cuvette error comes from the cuvette holder not being able to lock the cuvette in place, like in a commercial instrument. Data was collected using a custom-built fluorescence detection system, and the cuvette

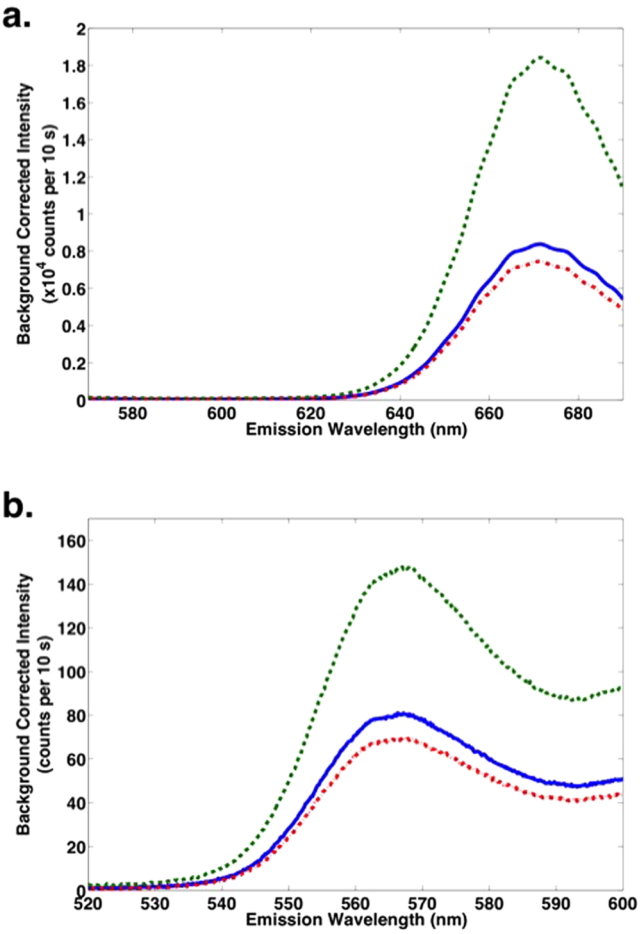

Figure 2. Fluorescence emission from the reporter started at about 530 nm and went to approximately 690 nm. (a) Cy5 emission ranged from 620 to 690 nm. (b) Cy3 emission went from 540 to 590 nm. (blue line) = 1 μM reporter, (green dash) = 1 μM reporter-probe1 complex, and (red dash-dot) = 1 μM reporter-probe1 plus 1 μM target. The reporter was excited with 742 nm at ∼100 mW.

holder was made in our machine shop. The system used to collect fluorescence is only used to characterize and validate biosensor efficacy prior to cell and tissue applications. Future studies will use an average background signal that accounts for changes in cuvette placement.

For the remainder of the discussion, the region of the spectrum where Cy5 emits (620−690 nm, Figure 2a) will be referred to as the Cy5 emission region. The region of the spectrum where Cy3 emits (540−590 nm, Figure 2b) will be referred to as the Cy3 emission region. As demonstrated in Figure 2, addition of probe causes the reporter signal to increase as the hairpin unfolds and moves the Cy3 and Cy5 away from one another. When Let-7a is added, the fluorescence decreases back to the original value. From these observations, we hypothesize the Cy3 and some of the nucleic acids are causing the emission from the Cy5 to decrease when the reporter is in the hairpin configuration. To test this hypothesis, we conducted two studies that compared the percent decrease in the fluorescence of Cy5 when in proximity to either nucleic acids or Cy3. These studies used hairpin and linear reporters. Table 1 and Table S1, Supporting Information, lists the oligonucleotide sequences used in the study. A reporter that lacked Cy3 on the 3-prime end was obtained and used to compare to the reporter with Cy3 on the 3-prime end. Three

dx.doi.org/10.1021/ac403866g | Anal. Chem. 2014, 86, 1853−1863

linear reporters were purchased; one had Cy5 on the 5-prime end, while the complementary strand was labeled with or without Cy3 at the 3-prime end of the oligonucleotide.

Figure 3 compares the average decrease in signal of the reporter-probe complex with and without Cy3 on the 3-prime end of the reporter upon probe-Let-7a binding. The reporter with Cy3 and Cy5 causes the signal to decrease by 57.7 ± 1.9% (N = 3) after addition of Let-7a. The reporter without the Cy3 only results in a 32.6 ± 2.4% (N = 3) decrease in signal. Addition of Cy3 provides an additional 25.1 ± 3.1% contribution to the decrease in signal when the reporter changes configuration after releasing the probe. Comparing the means shows that at the 99% confidence interval the means are statistically different and we conclude that Cy3 adds a statistically significant improvement to the dynamic range of the signal change.

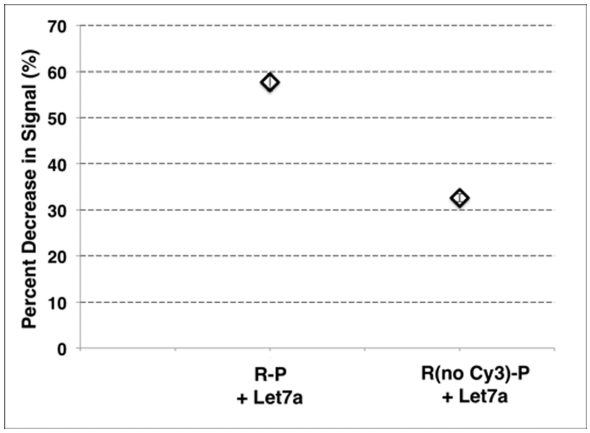

Figure 3. Comparison of observed fluorescence quenching of a 5-prime-Cy5-reporter with and without Cy3 at the 3-prime end. Displayed as percent decrease in signal. R-P = reporter-probe1 complex. Error bars for N = 3 are the same size as the symbols. Samples were excited with 742 nm at 100 mW.

To further confirm Cy3 and nucleic acid proximity contributes to Cy5 quenching, we conducted studies using a 22 nucleic acid long linear oligonucleotide labeled with Cy5 on the 5 prime end. In these experiments, linear strands of 5-prime Cy5 were exposed to buffer, noncomplementary DNA, complementary DNA with No Cy3, and a complementary DNA labeled with Cy3 on the 3-prime end. Nucleic acids alone decrease the Cy5 signal by 44.8 ± 2.0% (N = 4). The Cy3 contributes an additional 29.2 ± 2.5% to the decrease in signal (Figure S3, Supporting Information). Addition of noncomplementary DNA oligonucleotide showed no decrease in signal, confirming only complementary binding of nucleic acids contributes to observed decrease in Cy5 signal. Using noncomplementary DNA provides a negative control to confirm nucleic acids must be close to the Cy5 in order to decrease the emission (Figure S3, Supporting Information). From these experiments, we conclude the Cy5 is interacting with any of the four nucleic acids and the Cy3. Both studies demonstrate the Cy3 provides an additional 30% decrease in signal. It is likely that different combinations of adenine (A), thymine (T) and cytosine (C), and guanine (G) lead to different extents of quenching. Further studies will be needed to resolve the nature of the observed quenching from nucleic acids. We are currently exploring use of a quencher, Iowa Black, to further improve quenching. We hypothesize a quencher like Iowa Black will have more quenching of Cy5 than the Cy3-Cy5 pair. We further hypothesize that more quenching will lead to lower limits of detection and/or better signal resolution between different concentrations. From our preliminary data, we are finding that using the Iowa Black quencher reduces the signal by an additional ∼33%, improving the total quenching to ∼89% when the reporter is in the hairpin configuration.

Excitation Spectra of Reporter. Figure 4 shows the excitation spectra of the reporter with and without probe1. The excitation wavelength varied from 742 to 1032 nm (specifically 742, 782, 832, 862, 932, 992, and 1032 nm) with a constant power of 100 mW. The background corrected averaged summed intensity of the Cy3 and Cy5 emission regions were plotted as a function of excitation wavelength (Figure 4). The Cy3 and Cy5 dyes were chosen for their potential to demonstrate Förster resonance energy transfer (FRET). However, as demonstrated in Figure 4, no excitation wavelength was capable of producing FRET enhancement when the reporter is in the hairpin configuration. Instead, the excitation study revealed that, at each excitation wavelength, the hairpin configuration of the reporter had less emission intensity than the "open" reporter-probe1 configuration. Excitation at 742 nm was found to be the wavelength that had the largest change in analytical

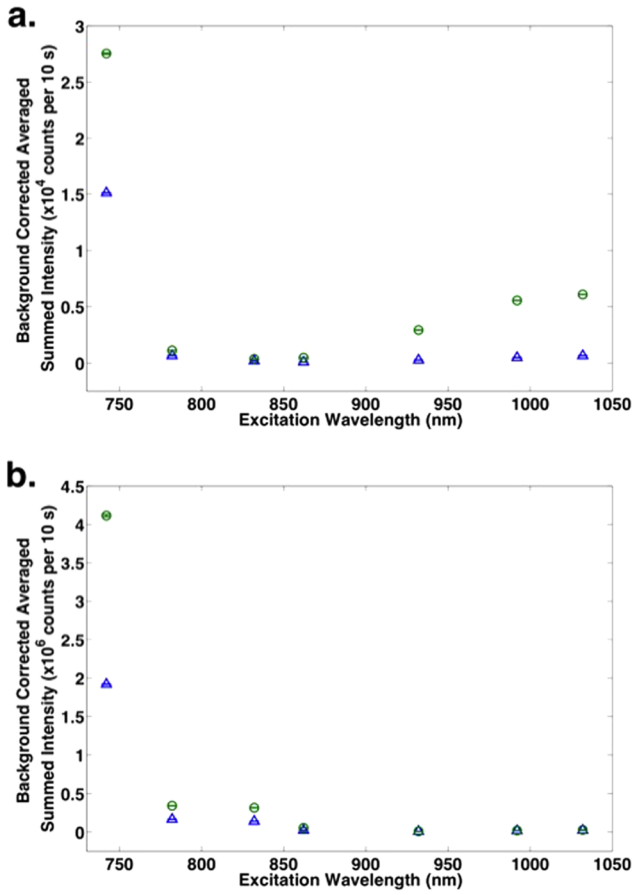

Figure 4. Excitation spectra of 1 μM reporter with and without 1 μM probe1. Excitation wavelength varied from 742 to 1032 nm at constant excitation power of approximately 100 mW. (a) Excitation spectra obtained by observing emission in the Cy3 region. (b) Excitation spectra obtained by observing emission in the Cy5 region. Error bars from 5 replicates are the same size or smaller than the symbols (blue triangles = reporter; green circles = reporter-probe1).

dx.doi.org/10.1021/ac403866g | Anal. Chem. 2014, 86, 1853−1863

signal for both dyes. From this observation, we decided to use 742 nm excitation for the remainder of the studies.

Nonlinear absorption characteristics of the reporter and the reporter-probe1 complex were investigated by increasing the excitation power from 25 to 200 mW in 25 mW steps. After processing data in Matlab, log−log plots of emission intensity vs average excitation power were prepared (data not shown). From these experiments, only the Cy3 showed nonlinear absorption over the 25 to 75 mW average power range. The hairpin configuration demonstrated three-photon absorption, but the reporter-probe1 complex demonstrated two-photon absorption. Both the hairpin and reporter-probe1 complex demonstrated a mixture of single- and two-photon absorption with excitation powers over 75 mW. Cy5 emission demonstrated single-photon absorption in both the hairpin and reporter-probe1 complex over the entire excitation power range from 25 to 200 mW. The deviations from expected two-photon observation most likely resulted from interactions between Cy3 and Cy5 and/or between the dyes and the nucleic acids. Future studies are planned to examine the photon absorption and emission characteristics of these dyes in more detail and are beyond the scope of this preliminary report on the biosensor.

Binding Kinetics and Analytical Signal Dynamics. Signal change, binding kinetics, signal stability, and specificity of the biosensor were investigated before and after addition of probe1. These studies were then applied to the reporter-probe1 complex before and after addition of Let-7a, noncomplementary miR-9, or a three nucleotide variant of the Let-7a (Let-7aV). Table 1 lists the sequences and predicted thermodynamics for each type of miRNA. For each sample, fluorescence was observed for 1 min time intervals over a 30 min time period (each time interval was spaced by 5 min). These experiments were repeated four times to demonstrate and establish stability and reproducibility of the signal. The biosensor exhibited a signal stability of about 2−5% over a 30 min time period. The excitation beam was blocked in-between measurement time points to prevent photodamage of the oligonucleotides and dyes.

The length of time needed for hybridization of reporter-probe1 was determined by monitoring changes in Cy5 fluorescence over time after addition of probe1 to the reporter. Figure 5 shows an overlay of the background corrected averaged summed intensity (N = 4) of Cy5 before and after addition of probe1 to the reporter. The solutions contained 1 μM reporter (blue circles) and 833 nM reporter plus 833 nM probe1 (green circles). The reporter signal is reproducible and stable at about $1.88 \times 10^6 \pm 0.05 \times 10^6$ (N = 5) counts per 10 s over a 24 min time period (Figure 5). The first datum for the reporter plus probe1 hybridization experiment was taken within 1 min after adding probe1 to the reporter. The time it takes for the signal to stabilize after addition of probe1 was used as a metric to determine hybridization time. According to Figure 5, the reporter-probe1 hybridization process takes about 6 min. After 6 min, the reporter-probe1 complex signal is reproducible and stable at $3.65 \times 10^6 \pm 0.17 \times 10^6$ (N = 4) counts per 10 s. The increase in signal observed in Figure 5 after addition of probe1 to reporter provides convincing evidence that the signal change can be related to probe addition. In the Cy3 emission region (data not shown), three of the four replicates took about 20 min for the signal to stabilize. However, one of the four replicates took only 5 min to stabilize. After 45 min (data not shown), the error in the signal from both the Cy3 and Cy5 emission was about 4% (N = 4). From these studies, we decided a 20 min hybridization period should be used to form the reporter-probe1 complex.

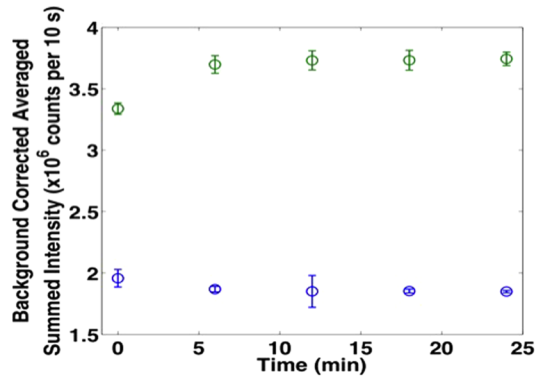

Figure 5. Background corrected averaged summed Cy5 intensity (N = 4) time trace of 1 μM reporter before probe1 addition (blue circles) and 833 nM reporter and probe1 (green circles) after probe addition. Error bars from 4 replicate measurements are the same size or smaller than the symbols. Both solutions were excited with 742 nm at 100 mW average power.

The specificity of the reporter-probe1 complex for Let-7a was investigated. In order to correlate the changes in the signal to a specific reagent being added, each experiment started with the reporter alone and then different reagents were added directly to the cuvette prior to analysis. Each experiment started by monitoring the signal stability of 1 μM reporter over time. Probe1 was added to the reporter and allowed to incubate for 20 min in the cuvette with the laser beam blocked. The final concentration was 833 nM probe1 and 833 nM reporter. Then, the signal stability was monitored over 36 min. Finally, either target Let-7a or noncomplementary miR-9 was added to the cuvette containing the reporter-probe1 complex. A 10 min incubation period was used for addition of target or noncomplementary miRNA, with the laser beam blocked during incubation. The final concentration was 750 nM Let-7a target or noncomplementary miR-9, 750 nM probe1, and 750 nM reporter. The signal stability was monitored for 30 min.

As different oligonucleotides were sequentially added to a solution containing the reporter, a dynamic change in signal is observed (Figure 6). Because probe1, target Let-7a, and noncomplementary miR-9 were added to the reporter solution *in situ*, dilution effects on the signal had to be taken into account (blue circles). Addition of probe1 results in more than doubling of signal for both dyes (compare reporter plus buffer to reporter plus probe1 at minute 73, in Figure 6). Addition of the Let-7a to the reporter-probe1 complex resulted in the signal decreasing to approximately the same value as reporter alone, with dilution taken into account (compare minute 120 for reporter plus buffer to reporter plus probe1 plus target, in Figure 6).

Slight fluctuation in the signal is observed over the 73 to 109 min and the 120 to 150 min time intervals. Variation in signal corresponded to about a 1−2% relative standard deviation over the two time intervals. These fluctuations could be attributed to binding stability and/or photobleaching. Photobleaching was observed for the earlier binding kinetic studies, but the effects on signal were minor (data not shown). Future studies will use lower excitation powers to reduce photobleaching and other photodamaging effects. The difference between the green triangles and red plus symbols in Figure 6a over the first 109 min is most likely a result of cuvette placement error. Notice

dx.doi.org/10.1021/ac403866g | *Anal. Chem.* 2014, 86, 1853−1863

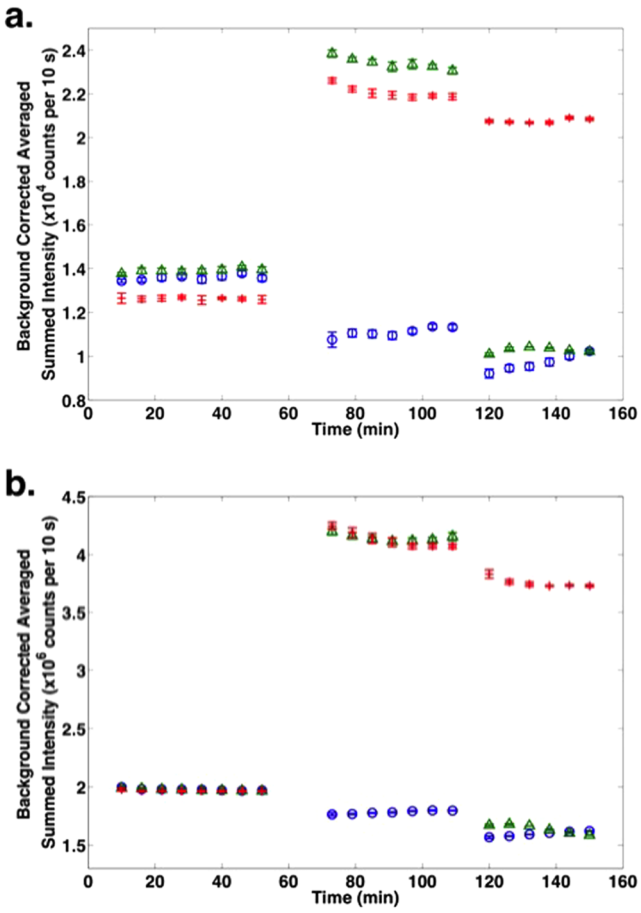

Figure 6. Background corrected averaged (N = 6) summed intensity of reporter from (a) Cy3 and (b) Cy5. Over time, diluent, probe1, target Let-7a, or noncomplementary miR-9 was added. The change in signal from minute 52 to minute 73 confirms reporter-probe1 complexation. The change in signal from minute 109 to minute 120 confirms specificity of the reporter-probe1 complex for the target of interest. Blue circles, reporter plus buffer dilution controls; green triangles, reporter plus probe1 plus Let-7a; red pluses, reporter plus probe1 plus noncomplementary miR-9. Samples were excited with 742 nm at ~100 mW. Error bars from 6 replicates are the same size or smaller than the symbols.

this difference was negligible in Figure 6b. In general, the instrumental error was around 1%. The signal stability of the reporter-probe complex is around 1−4%. We found the dominant source of variability in our measurements is cuvette placement error, with this error varying between 1% and 10%.

A nonspecific binding study demonstrated the ability of the sensor to distinguish Let-7a target (green triangles) from noncomplementary miR-9 (red plus). The small decrease in signal observed in Figure 6 upon addition of miR-9 (compare minute 109 to minute 120) was expected from the dilution factor. A 10% decrease in signal was expected from dilution of the reporter-probe1 complex. Adding miR-9 only decreased the signal by 6% ± 2% (N = 6) in the Cy3 emission region and by 9% ± 2% (N = 6) in the Cy5 emission region.

We further evaluated the specificity of the biosensor by presenting it with a miRNA that was nearly identical to the Let-7a except three nucleic acids were changed. Figure 7 compares the percent decrease in Cy5 signal upon addition of different types of miRNA to the reporter-probe complex. The values presented in Figure 7 take the dilution factor into account when

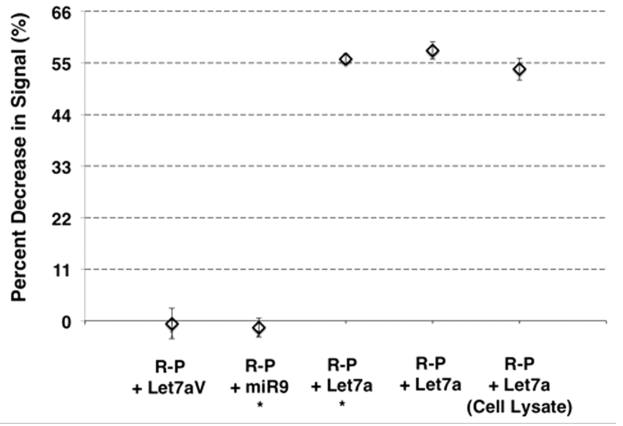

Figure 7. Comparison of observed percent decrease of reporter Cy5 emission to evaluate specificity, stability, and effects of cell lysate on reporter-probe biosensor. Displayed as percent decrease in signal. R-P = reporter-probe1 complex. Unless otherwise stated, all solutions were prepared in buffer. Some error bars are the same size as the symbol. The ∗ indicates N = 6 and the long-term study, otherwise N = 3; each replicate consisted of a 1000 ms exposure time that was averaged over 10 spectra to enhance the signal-to-noise.

determining the percent decrease in signal. A three nucleotide Let-7a variant (Let-7aV) demonstrated a −0.6 ± 3.3% (N = 3) change in signal. Addition of the miR-9 showed a −1.6 ± 2.0% (N = 6) change in signal. The negative sign here indicates the signal increases slightly but is not statistically different from 0% change. Addition of the Let-7a target resulted in a decrease in signal of ~57%. These results provide further evidence that the biosensor design has great potential as a selective biosensor.

The long-term stability of the biosensor can also by seen in Figure 7 (indicated by the ∗ under the data point label). The response of biosensor over a four month time period was statistically similar at the 99% confidence interval. At month one, the percent decrease in signal from Let-7a addition was 55.8 ± 1.1% (N = 6), and it was 57.7 ± 1.9% (N = 3) at month four. The biosensor is stable for at least four months. For this case, the instrument response error and the cuvette placement error are similar. During the four months of storage, the reporter and probe were stored separately at a concentration of 100 μM in RNase/DNase free 18-MΩ water at −20 °C. When reporter-probe biosensor was to be used, the reporter and probe were first individually diluted to a concentration of 10 μM in the dilution buffer. The reporter and probe were then hybridized together at the desired concentration (1 μM or 100 nM) prior to presenting miRNAs to the reporter-probe complex.

The signal response of the biosensor in cell lysate was studied to determine if proteins, DNA, and other RNA species found in a cell will cause interference in the measurement of Let7a. Raw cell lysate was diluted in half with buffer to lower the concentration of potential interfering species. Determinations of protein and oligonucleotide concentrations were made on the Nanodrop using 280 and 260 nm, respectively. The concentration of DNA and RNA species in cell lysate was ~30 times greater than the amount of reporter-probe complex and Let-7a. The amount of protein in the cell lysate was ~480 times more concentrated than the reporter-probe complex and Let-7a. Cell lysate solutions were used to prepare the reporter-probe biosensor and to test the recognition and transduction mechanism. A comparison of percent decrease in Cy5 signal

dx.doi.org/10.1021/ac403866g | Anal. Chem. 2014, 86, 1853−1863

from the biosensor in clean buffer and in cell lysate environments is presented in Figure 7. Cell lysate reduced the signal by 53.7 ± 2.4% (N = 3) compared to 57.7 ± 1.9% (N = 3) in the clean buffer. At the 99% confidence interval, these values are not statistically different. This result indicates components in the cell lysate do not have an observable effect on the percent decrease in signal upon addition of Let-7a. Furthermore, the reporter-probe biosensor demonstrates great potential for *in vivo* applications.

Sensitivity. The limits of detection, limits of quantitation, and sensitivity of the biosensor at 1 μM and 100 nM concentration levels were evaluated and presented in Table 2.

Table 2. Analytical Figures of Merit Describing Sensitivity of Reporter-Probe Biosensor for Let-7a

	100 nM Reporter-Probe[a]	1 μM Reporter-Probe
Detection Limit (nM)	4 (±1)	9 (±4)
Quantitation Limit (nM)	16 (±2)	18 (±4)
Sensitivity (counts/nM)	3.6×10^5 ($\pm 0.23 \times 10^5$)	9.5×10^4 ($\pm 0.1 \times 10^4$)
Linear Dynamic range (nM)	4−100	9−1000
Signal to Noise (S/N) at zero analyte addition	1047	1601

[a]Exposure time for 100 nM reporter-probe was 500 ms instead of 100 ms for the 1 μM reporter-probe complex.

Statistical analysis of the calibration studies suggests the 1 μM reporter-probe1 biosensor has a limit of detection and quantitation of 9 ± 4 nM (N = 3) and 18 ± 4 nM (N = 3), respectively. Making a crude estimation of the focal volume to be around 1 μL and considering 9 femtomoles of Let-7a, at the detection limit, and 1 picomole from the 1 μM reporter-probe1 complex, we find ∼100 times more fluorescent species than quenched-fluorescent species. To determine if this was a limiting factor on the detection limit, a 100 nM solution of reporter-probe1 complex will decrease the number of fluorescent to quenched-fluorescent species by a factor of 10 and perhaps the limit of detection will be lowered.

Reducing the reporter-probe concentration to 100 nM yields 4 ± 1 nM (N = 3) and 16 ± 1 nM (N = 3) for limits of detection and quantitation, respectively. The sensitivity of the 1 μM reporter-probe1 biosensor to the Let-7a was around 9.5×10^4 counts/nM. Increasing the exposure time to 500 ms for the 100 nM reporter-probe1 biosensor resulted in a sensitivity of 3.6×10^5 counts/nM. The dynamic range of the concentration was approximately 10^2 orders of magnitude for both concentrations of reporter-probe1 complex. There was a relatively small ∼0.4% error between the zero analyte addition and the y-intercept for both concentrations of reporter-probe1 biosensor. This error was propagated into the precision of the quantitation limit. The precision of the LOQ for the 1 μM and 100 nM reporter-probe1 biosensor was 22% and 12%, respectively. Precision in the limit of quantitation in the signal was less than 1%. Considering excellent precision in the signal limit of quantitation, we suspect pipetting errors were the major source of error in determination of the limits of detection and quantitation.

Decreasing the reporter-probe1 concentration by a factor of 10 has a marginal impact on the limits of detection and quantitation; however, the precision was improved by a factor of 2. Given the signal-to-noise is on the order of 10^3 for the 100 nM reporter-probe1 complex with zero analyte addition, it is possible the reporter-probe1 concentration can be decreased by at least 2 orders of magnitude to picomolar levels. Assuming a similar concentration dynamic range, it is possible that picomolar limits of detection can be achieved for target miRNA. Use of quenchers and signal-on approaches are currently being investigated to improve the analytical figures of merit.

Reporter Specificity. Noncomplementary Let-7a and miR-9 were added to a solution containing the reporter to test the specificity of the reporter for the probe. Minor nonspecific binding of Let-7a to the reporter was noticed in the Cy3 emission region (∼30%) but not in the Cy5 emission region. Addition of miR-9 exhibited about 17% nonspecific binding to reporter in both the Cy3 and Cy5 emission regions. Future experiments will focus on redesigning the reporter to minimize nonspecific binding effects to a negligible amount.

False Positives from Endonuclease Degradation. Enzymatic degradation from nucleases remains a problem plaguing oligonucleotide-based biosensors. The reporter-probe biosensor was designed specifically to address this problem. Nuclease degradation studies were performed to demonstrate the reduced false positives of the reporter-probe biosensor compared to other biosensors. For these experiments, a reporter-probe biosensor, a molecular beacon, and a traditional double-strand displacement biosensor were subjected to nuclease degradation. Table 1 provides the sequences and thermodynamic information for the various types of biosensors. The double-strand displacement biosensor used a Cy3-Cy5 dye pair for signal transduction. The molecular beacon used a Cy5 reporting dye and an Iowa Black quencher for signal transduction. Equations 1, 2, and 3 were used to determine the percent change in signal due to enzyme degradation:

$$\%\Delta I_{RP} = 100 \times \frac{I_{RP+Enzyme} - I_{Reporter}}{I_{RP} - I_{Reporter}} \quad (1)$$

$$\%\Delta I_{MB} = 100 \times \frac{I_{MB+Enzyme} - I_{MB}}{I_{MB+Target} - I_{MB}} \quad (2)$$

$$\%\Delta I_{DSD} = 100 \times \frac{I_{DSD+Enzyme} - I_{DSD}}{I_{Cy5} - I_{DSD}} \quad (3)$$

% ΔI_{RP}, % ΔI_{MB}, and % ΔI_{DSD} are the percent changes in signal of the reporter-probe biosensor, the molecular beacon, and the double-strand displacement biosensor, respectively. The numerator corresponds to the change in signal from addition of enzyme; the denominator corresponds to the dynamic range of the biosensors.

Both the molecular beacon and the reporter-probe biosensor have LNA modifications. The molecular beacon showed the most false positive error with a 62% ± 2% (N = 3) change in signal. The reporter-probe1 complex showed reduced false positives with only a 47% ± 1% (N = 3) change in signal. This false positive resulted from the stems of the reporter not being thoroughly degraded by the endonuclease. The stems of the reporter in the reporter-probe1 complex were not digested because endonucleases do not effectively react with single-stranded oligonucleotides. As a result, the stems survived endonuclease treatment and were able to rebind and cause a false change in the analytical signal. These results demonstrate that even with LNA both molecular beacons and the reporter-probe1 biosensor are susceptible to false positives. However, the reporter-probe1 demonstrates promise to reduce the extent of false positives. The double-strand displacement biosensor showed a false positive error of 27% ± 1% change in signal.

dx.doi.org/10.1021/ac403866g | Anal. Chem. 2014, 86, 1853−1863

To solve the false positive problem with probe1, a different probe was designed. Probe2 was designed to bind the stems of the reporter and force the endonuclease to degrade those regions as well. The reporter-probe2 complex showed no false positives. In fact, the percent change in signal was −25% ± 5%. The negative percent change in signal from reporter-probe2 is attributed to residual quenching of Cy5 from nucleic acids and Cy3 on the reporter-probe2 complex. Therefore, degradation of the reporter-probe2 complex will cause the Cy3 and Cy5 to move apart, disrupting any quenching and increasing the Cy5 signal. Since the reporter-probe complex works as a signal-off sensor, the increase in signal will not contribute to a false positive. Future reporter designs will add carbon-based spacer moieties to increase the distance between dyes and nucleic acids. Future probe designs will only bind one of the stems to improve displacement kinetics and reduce false negatives. The overall aim will be to redesign the reporter-probe complex to reduce false negatives and false positives to a negligible amount. Adding spacers will have an additional benefit of reducing other forms of nonradiative quenching when the reporter hairpin configuration is formed. Signal-on techniques are more desirable for *in situ* analysis so we are also currently exploring other resonance energy transfer pairs so the signal will turn on when the reporter folds into the hairpin configuration.

CONCLUSION

Early onset of disease can be detected by monitoring changes in miRNA expression levels. This information can be used to initiate timely treatment and/or develop customized treatments for specific diseases. The reporter-probe biosensor has potential to be implemented into existing miRNA therapeutics to serve as a simple indirect indicator of miRNA drug-target binding. The speed, sensitivity, selectivity, and reduced false positive characteristics of the reporter-probe biosensor make it an attractive alternative over current biosensors for miRNA analysis. Low nanomolar limits of detection and a sensitivity of 10^5 counts/nM were observed for the reporter-probe biosensor. Given the analytical figures of merit, we anticipate that reduction of reporter-probe concentration by 2 to 3 orders of magnitude will improve our detection limits by a corresponding amount.

With the commercial availability of designer oligonucleotides, the reporter-probe biosensor can be reconfigured so it is selective for any RNA or DNA of interest. Using cell membrane transport methods currently employed for molecular beacons, the reporter-probe biosensor has potential for *in situ* cellular analysis. The ability of the reporter-probe biosensor to reduce false positives gives it a conceivable advantage when used for *in situ* applications due to the abundance of nucleases within cells. We have established the foundation for a new class of displacement biosensors that use reporter-probe complexes; future studies will focus on optimization of the recognition and transduction mechanisms to increase selectivity and sensitivity.

ASSOCIATED CONTENT

Supporting Information

Additional information as noted in text. This material is available free of charge via the Internet at http://pubs.acs.org.

AUTHOR INFORMATION

Corresponding Author

*E-mail: sean.burrows@oregonstate.edu.

Author Contributions

The manuscript was written through contributions of all authors. All authors have given approval to the final version of the manuscript.

Notes

The authors declare no competing financial interest.

ACKNOWLEDGMENTS

This work was funded by Oregon State University.

REFERENCES

(1) Volinia, S.; Calin, G. A.; Liu, C.-G.; Ambs, S.; Cimmino, A.; Petrocca, F.; Visone, R.; Iorio, M.; Roldo, C.; Ferracin, M.; Prueitt, R. L.; Yanaihara, N.; Lanza, G.; Scarpa, A.; Vecchione, A.; Negrini, M.; Harris, C. C.; Croce, C. M. *Proc. Natl. Acad. Sci. U. S. A.* **2006**, *103*, 2257−2261.

(2) Zhu, S.; Wu, H.; Wu, F.; Nie, D.; Sheng, S.; Mo, Y.-Y. *Cell Res.* **2008**, *18*, 350−359.

(3) Iorio, M. V.; Ferracin, M.; Liu, C.-G.; Veronese, A.; Spizzo, R.; Sabbioni, S.; Magri, E.; Pedriali, M.; Fabbri, M.; Campiglio, M. *Cancer Res.* **2005**, *65*, 7065−7070.

(4) Mitomo, S.; Maesawa, C.; Ogasawara, S.; Iwaya, T.; Shibazaki, M.; Yashima-Abo, A.; Kotani, K.; Oikawa, H.; Sakurai, E.; Izutsu, N.; Kato, K.; Komatsu, H.; Ikeda, K.; Wakabayashi, G.; Masuda, T. *Cancer Sci.* **2008**, *99*, 280−286.

(5) Visone, R.; Russo, L.; Pallante, P.; Martino, I. D.; Ferraro, A.; Leone, V.; Borbone, E.; Petrocca, F.; Alder, H.; Croce, C. M.; Fusco, A. *Endocr. Relat. Cancer* **2007**, *14*, 791−798.

(6) Akao, Y.; Nakagawa, Y.; Naoe, T. *Oncol. Rep.* **2006**, *16*, 845−850.

(7) Shi, B.; Sepp-Lorenzino, L.; Prisco, M.; Linsley, P.; deAngelis, T.; Baserga, R. *J. Biol. Chem.* **2007**, *282*, 32582−32590.

(8) Sylvestre, Y.; Guire, V. D.; Querido, E.; Mukhopadhyay, U. K.; Bourdeau, V.; Major, F.; Ferbeyre, G.; Chartrand, P. *J. Biol. Chem.* **2007**, *282*, 2135−2143.

(9) Shi, X.-B.; Xue, L.; Yang, J.; Ma, A.-H.; Zhao, J.; Xu, M.; Tepper, C. G.; Evans, C. P.; Kung, H.-J.; White, R. W.; deVere. *Proc. Natl. Acad. Sci. U. S. A.* **2007**, *104*, 19983−19988.

(10) Johnson, S. M.; Grosshans, H.; Shingara, J.; Byrom, M.; Jarvis, R.; Cheng, A.; Labourier, E.; Reinert, K. L.; Brown, D.; Slack, F. J. *Cell* **2005**, *120*, 635−647.

(11) Fabbri, M.; Garzon, R.; Cimmino, A.; Liu, Z.; Zanesi, N.; Callegari, E.; Liu, S.; Alder, H.; Costinean, S.; Fernandez-Cymering, C.; Volinia, S.; Guler, G.; Morrison, C. D.; Chan, K. K.; Marcucci, G.; Calin, G. A.; Huebner, K.; Croce, C. M. *Proc. Natl. Acad. Sci. U. S. A.* **2007**, *104*, 15805−15810.

(12) Shell, S.; Park, S.-M.; Radjabi, A. R.; Schickel, R.; Kistner, E. O.; Jewell, D. A.; Feig, C.; Lengyel, E.; Peter, M. E. *Proc. Natl. Acad. Sci. U. S. A.* **2007**, *104*, 11400−11405.

(13) Giannakakis, A.; Sandaltzopoulos, R.; Greshock, J.; Liang, S.; Huang, J.; Hasegawa, K.; Li, C.; O'Brien-Jenkins, A.; Katsaros, D.; Weber, B. L.; Simon, C.; Coukos, G.; Zhang, L. *Cancer Biol. Ther.* **2008**, *7*, 255−264.

(14) Ikeda, S.; Kong, S. W.; Lu, J.; Bisping, E.; Zhang, H.; Allen, P. D.; Golub, T. R.; Pieske, B.; Pu, W. T. *Physiol. Genomics* **2007**, *31*, 367−373.

(15) Fiore, R.; Siegel, G.; Schratt, G. *Biochim. Biophys. Acta, Gene Regul. Mech.* **2008**, *1779*, 471−478.

(16) Taganov, K. D.; Boldin, M. P.; Chang, K.-J.; Baltimore, D. *Proc. Natl. Acad. Sci. U. S. A.* **2006**, *103*, 12481−12486.

(17) Alhasan, A. H.; Kim, D. Y.; Daniel, W. L.; Watson, E.; Meeks, J. J.; Thaxton, C. S.; Mirkin, C. A. *Anal. Chem.* **2012**, *84*, 4153−4160.

(18) Chen, C.; Ridzon, D. A.; Broomer, A. J.; Zhou, Z.; Lee, D. H.; Nguyen, J. T.; Barbisin, M.; Xu, N. L.; Mahuvakar, V. R.; Andersen, M. R.; Lao, K. Q.; Livak, K. J.; Guegler, K. J. *Nucleic Acids Res.* **2005**, *33*, No. e179.

(19) Calin, G. A.; Liu, C.-G.; Sevignani, C.; Ferracin, M.; Felli, N.; Dumitru, C. D.; Shimizu, M.; Cimmino, A.; Zupo, S.; Dono, M.; Dell'Aquila, M. L.; Alder, H.; Rassenti, L.; Kipps, T. J.; Bullrich, F.;

Negrini, M.; Croce, C. M. *Proc. Natl. Acad. Sci. U. S. A.* **2004**, *101*, 11755−11760.
(20) Liu, C.-G.; Calin, G. A.; Meloon, B.; Gamliel, N.; Sevignani, C.; Ferracin, M.; Dumitru, C. D.; Shimizu, M.; Zupo, S.; Dono, M.; Alder, H.; Bullrich, F.; Negrini, M.; Croce, C. M. *Proc. Natl. Acad. Sci. U. S. A.* **2004**, *101*, 9740−9744.
(21) Thomson, J. M.; Parker, J.; Perou, C. M.; Hammond, S. M. *Nat. Methods* **2004**, *1*, 47−53.
(22) Várallyay, É.; Burgyán, J.; Havelda, Z. *Nat. Protoc.* **2008**, *3*, 190−196.
(23) Valoczi, A.; Hornyik, C.; Varga, N.; Burgyan, J.; Kauppinen, S.; Havelda, Z. *Nucleic Acids Res.* **2004**, *32*, No. e175.
(24) Calin, G. A.; Sevignani, C.; Dumitru, C. D.; Hyslop, T.; Noch, E.; Yendamuri, S.; Shimizu, M.; Rattan, S.; Bullrich, F.; Negrini, M.; Croce, C. M. *Proc. Natl. Acad. Sci. U. S. A.* **2004**, *101*, 2999−3004.
(25) Vieregg, J. R.; Nelson, H. M.; Stoltz, B. M.; Pierce, N. A. *J. Am. Chem. Soc.* **2013**, *135*, 9691−9699.
(26) Tyagi, S.; Kramer, F. R. *Nat. Biotechnol.* **1996**, *14*, 303−308.
(27) Conlon, P.; Yang, C. J.; Wu, Y.; Chen, Y.; Martinez, K.; Kim, Y.; Stevens, N.; Marti, A. A.; Jockusch, S.; Turro, N. J.; Tan, W. *J. Am. Chem. Soc.* **2008**, *130*, 336−342.
(28) Tan, X.; Chen, W.; Lu, S.; Zhu, Z.; Chen, T.; Zhu, G.; You, M.; Tan, W. *Anal. Chem.* **2012**, *84*, 8272−8276.
(29) Yao, Q.; Zhang, A.; Ma, H.; Lin, S.; Wang, X.; Sun, J.; Chen, Z. *Mol. Cell. Probes* **2012**, *26*, 182−187.
(30) Tsourkas, A.; Behlke, M. A.; Xu, Y.; Bao, G. *Anal. Chem.* **2003**, *75*, 3697−3703.
(31) Santangelo, P. J.; Nix, B.; Tsourkas, A.; Bao, G. *Nucleic Acids Res.* **2004**, *32*, No. e57.
(32) King, F. W.; Liszewski, W.; Ritner, C.; Bernstein, H. S. *Stem Cells Dev.* **2011**, *20*, 475−484.
(33) Mergny, J. L.; Boutorine, A. S.; Garestier, T.; Belloc, F.; Rougee, M.; Bulychev, N. V.; Koshkin, A. A.; Bourson, J.; Lebedev, A. V.; Valeur, B. *Nucleic Acids Res.* **1994**, *22*, 920−928.
(34) Tsuji, A.; Sato, Y.; Hirano, M.; Suga, T.; Koshimoto, H.; Taguchi, T.; Ohsuka, S. *Biophys. J.* **2001**, *81*, 501−515.
(35) Tsuji, A.; Koshimoto, H.; Sato, Y.; Hirano, M.; Sei-Iida, Y.; Kondo, S.; Ishibashi, K. *Biophys. J.* **2000**, *78*, 3260−3274.
(36) Sau, S. P.; Kumar, P.; Sharma, P. K.; Hrdlicka, P. J. *Nucleic Acids Res.* **2012**, *40*, No. e162.
(37) Sau, S. P.; Hrdlicka, P. J. *J. Org. Chem.* **2012**, *77*, 5−16.
(38) Bag, S. S.; Kundu, R.; Jana, S. *Tetrahedron Lett.* **2013**, *54*, 2627−2632.
(39) Baker, B. A.; Mahmoudabadi, G.; Milam, V. T. *Colloids Surf., B: Biointerfaces* **2013**, *102*, 884−890.
(40) Hemphill, J.; Deiters, A. *J. Am. Chem. Soc.* **2013**, *135*, 10512−10518.
(41) Prigodich, A. E.; Randeria, P. S.; Briley, W. E.; Kim, N. J.; Daniel, W. L.; Giljohann, D. A.; Mirkin, C. A. *Anal. Chem.* **2012**, *84*, 2062−2066.
(42) Wabuyele, M. B.; Vo-Dinh, T. *Anal. Chem.* **2005**, *77*, 7810−7815.
(43) Cao, Y. C.; Jin, R.; Mirkin, C. A. *Science* **2002**, *297*, 1536−1540.
(44) Pasquinelli, A. E.; Reinhart, B. J.; Slack, F.; Martindale, M. Q.; Kuroda, M. I.; Maller, B.; Hayward, D. C.; Ball, E. E.; Degnan, B.; Müller, P. *Nature* **2000**, *408*, 86−89.
(45) Pasquinelli, A. E.; McCoy, A.; Jiménez, E.; Salo, E.; Ruvkun, G.; Martindale, M. Q.; Baguna, J. *Evol. Dev.* **2003**, *5*, 372−378.
(46) Roush, S.; Slack, F. J. *Trends Cell Biol.* **2008**, *18*, 505−516.
(47) Reinhart, B. J.; Slack, F. J.; Basson, M.; Pasquinelli, A. E.; Bettinger, J. C.; Rougvie, A. E.; Horvitz, H. R.; Ruvkun, G. *Nature* **2000**, *403*, 901−906.
(48) Esquela-Kerscher, A.; Slack, F. J. *Nat. Rev. Cancer* **2006**, *6*, 259−269.
(49) Shi, X.-B.; Tepper, C. G.; deVere White, R. W. *Cell Cycle* **2008**, *7*, 1529−1538.
(50) Ingle, J. D.; Crouch, S. R. *Spectrochemical Analysis*; Prentice Hall: Upper Saddle River, NJ, 1988.
(51) Markham, N. R.; Zuker, M. *Nucleic Acids Res.* **2005**, *33*, W577−W581.
(52) Markham, N. R.; Zuker, M. In *Bioinformatics*; Keith, J. M., Ed.; Humana Press: Totowa, NJ, 2008; Vol. *453*, pp 3−31.
(53) DINAMelt mfold.rit.albany.edu [http://mfold.rna.albany.edu/?q=DINAMelt] (accessed Jun 20, 2013).
(54) Lennox, K. A.; Owczarzy, R.; Thomas, D. M; Walder, J. A.; Behlke, M. A. *Mol. Ther. Nucleic Acids.* **2013**, *2*, No. e117.
(55) Peng, Z.; Soper, S. A.; Pingle, M. R.; Barany, F.; Davis, L. M. *Anal. Chem.* **2010**, *82*, 9727−9735.
(56) Wabuyele, M. B.; Farquar, H.; Stryjewski, W.; Hammer, R. P.; Soper, S. A.; Cheng, Y.-W.; Barany, F. *J. Am. Chem. Soc.* **2003**, *125*, 6937−6945.